
3D-RFT: Reinforcement Fine-Tuning for Video-based 3D Scene Understanding

Xiongkun Linghu^{1*†} Jianguo Huang^{1,2*} Baoxiong Jia¹ Siyuan Huang¹

Abstract

Reinforcement Learning with Verifiable Rewards (RLVR) has emerged as a transformative paradigm for enhancing the reasoning capabilities of Large Language Models (LLMs), yet its potential in 3D scene understanding remains underexplored. Existing approaches largely rely on Supervised Fine-Tuning (SFT), where the token-level cross-entropy loss acts as an indirect proxy for optimization, leading to a misalignment between training objectives and task performances. To bridge this gap, we present Reinforcement Fine-Tuning for Video-based 3D Scene Understanding (3D-RFT), the first framework to extend RLVR to video-based 3D perception and reasoning. 3D-RFT shifts the paradigm by directly optimizing the model towards evaluation metrics. 3D-RFT first activates 3D-aware Multimodal Large Language Models (MLLMs) via SFT, followed by reinforcement fine-tuning using Group Relative Policy Optimization (GRPO) with strictly verifiable reward functions. We design task-specific reward functions directly from metrics like 3D IoU and F1-Score to provide more effective signals to guide model training. Extensive experiments demonstrate that 3D-RFT-4B achieves state-of-the-art performance on various video-based 3D scene understanding tasks. Notably, 3D-RFT-4B significantly outperforms larger models (*e.g.*, VG LLM-8B) on 3D video detection, 3D visual grounding, and spatial reasoning benchmarks. We further reveal good properties of 3D-RFT such as robust efficacy, and valuable insights into training strategies and data impact. We hope 3D-RFT can serve as a robust and promising paradigm for future development of 3D scene understanding. Code is available on [project page](#).

*Equal contribution ; †Project lead. ¹State Key Laboratory of General Artificial Intelligence, BIGAI ²Peking University. Correspondence to: Siyuan Huang <huangsiyuan@ucla.edu>, Baoxiong Jia <baoxiongjia@g.ucla.edu>.

1. Introduction

The remarkable success of MLLMs (Bai et al., 2025b;a; Hurst et al., 2024; Liu et al., 2023; Team et al., 2023; Comanici et al., 2025) has driven advancements in diverse fields, including 3D scene understanding (Huang et al., 2024b;a; Zhu et al., 2025a; Linghu et al., 2024; Zheng et al., 2025c;b), robotic manipulation (Driess et al., 2023; Brohan et al., 2023; Team et al., 2025a), and embodied navigation (Zheng et al., 2024; Zhang et al., 2024; Cheng et al., 2024a).

Treating 3D scenes as video streams offers a scalable alternative to traditional point-cloud and depth-based methods, bypassing the need for specialized sensors. By leveraging widely available RGB cameras and the temporal capabilities of MLLMs, this paradigm has become a central focus of recent research (Zheng et al., 2025c;b; Zhu et al., 2025a; Huang et al., 2025b; Fan et al., 2025). While some works (Zheng et al., 2025c; Zhu et al., 2025a) still inject explicit 3D features, others (Zheng et al., 2025b; Fan et al., 2025) extract 3D priors directly from video frames. Crucially, VG LLM (Zheng et al., 2025b) validates this approach on tasks like cross-frame detection and 3D visual grounding.

However, these approaches primarily rely on SFT as the learning paradigm, which imposes an inherent performance ceiling due to the limitations of answer-only supervision. Specifically, in 3D perception tasks, model responses consist of 3D bounding boxes represented as sequences of textual floating-point numbers. SFT optimizes these sequences via imitation learning, minimizing a per-token Cross-Entropy (CE) loss. This creates a critical misalignment: optimization occurs in the discrete token space, whereas evaluation is conducted in the continuous 3D coordinate system. Since the output tokens must be decoded and parsed into geometric structures to compute metrics like 3D Intersection over Union (IoU), the standard SFT objective acts only as an indirect proxy, failing to capture the true geometric quality of the predictions.

How can we overcome the inherent ceiling of answer-only supervision? RLVR offers a principled solution by optimizing models directly against **Verifiable Rewards**, which are derived directly from distinct evaluation metrics or pre-defined rules. Unlike SFT, which constrains the model to mimic ground-truth sequences via a per-token CE loss, Reinforcement Learning (RL) optimizes the policy based on

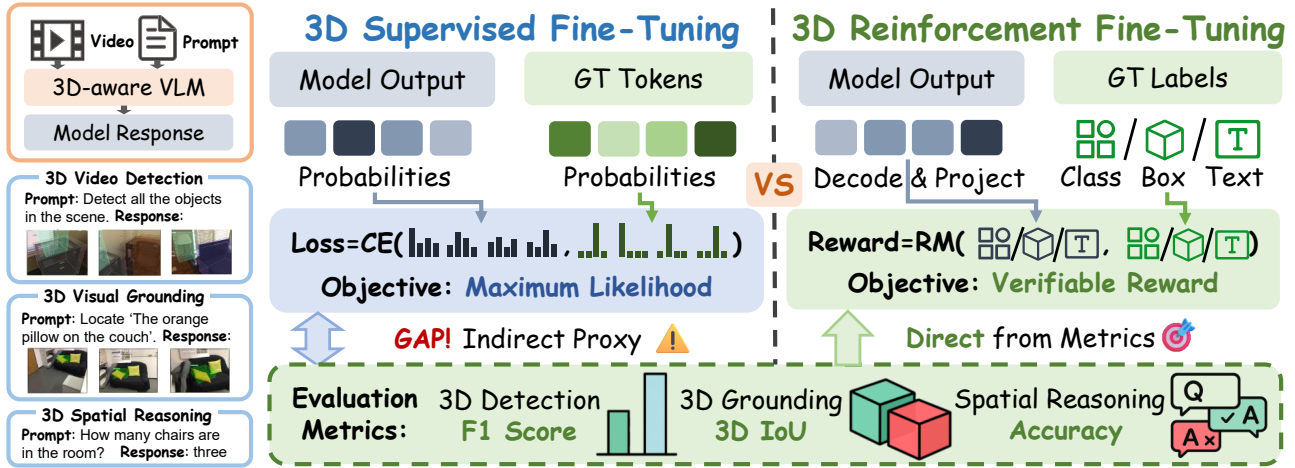


Figure 1. Comparison between SFT and 3D-RFT training paradigms. Left: Standard Supervised Fine-Tuning (SFT) relies on a per-token Cross-Entropy loss which acts as an indirect proxy, leading to a gap between training objectives and final evaluation metrics. Middle: Identical output formats for 3D Video Detection, Grounding, and Spatial Reasoning tasks. Right: 3D-RFT utilizes a Scalar Reward (Policy Gradient) derived directly from evaluation metrics (e.g., F1-Score, 3D IoU, and Accuracy) through a decoding and parsing module, ensuring the model directly optimizes for the final task performance.

scalar reward scores. This provides a superior optimization target that is strictly aligned with the evaluation process, encouraging sequence exploration without the limitations of token-level penalties. Recent breakthroughs, such as GPT-o1 (Jaech et al., 2024b) and DeepSeek-R1 (Guo et al., 2025), have widely demonstrated the success of RLVR in advancing mathematical reasoning and code generation.

A natural question arises: *Can this metrics-driven RL paradigm generalize to video-based 3D scene understanding?* To address this, we introduce 3D-RFT, a unified framework that successfully extends RL to diverse video-based 3D scene understanding tasks, encompassing both *3D perception* and *3D spatial reasoning*.

As illustrated in Fig. 1, 3D-RFT fundamentally shifts the training objective. While SFT relies on an indirect proxy—minimizing CE loss between predicted and ground-truth probabilities—this leads to a misalignment between training objectives and evaluation metrics. In contrast, 3D-RFT leverages policy gradients derived directly from verifiable reward signals (e.g., 3D IoU, Accuracy), ensuring the model is optimized explicitly for final task performance.

To overcome the lack of native 3D perception capabilities in existing MLLMs, we design a robust two-stage training pipeline: **1) SFT Warm-Up:** We first inject fundamental 3D awareness and scene understanding capabilities into the MLLM via SFT, establishing a stable policy initialization. **2) RL Training:** The model is then fine-tuned using the GRPO algorithm with verifiable reward functions strictly following evaluation protocols. For instance, in 3D Visual Grounding, we parse the predicted 9-DoF box, project it into the global coordinate system, and compute the global 3D IoU as the reward signal. This approach effectively tran-

sitions the learning paradigm from task-agnostic sequence imitation to metrics-driven policy optimization.

We validate the efficacy of 3D-RFT across typical video-based 3D scene understanding tasks, including 3D perception (e.g., 3D video detection (Wang et al., 2024), 3D visual grounding (Chen et al., 2020)) and 3D spatial reasoning (Yang et al., 2025a). Experimental results demonstrate that 3D-RFT consistently enhances model performance, and our model 3D-RFT-4B outperforms larger baseline models. Our analysis yields several key findings: 1) 3D-RFT provides consistent gains across all three task domains. 2) In 3D perception tasks, 3D-RFT significantly boosts performance over the SFT baseline, surpassing even 8B-scale fine-tuned models on nearly all metrics, proving that metrics-driven optimization offers a more effective learning objective. 3) For 3D spatial reasoning, 3D-RFT effectively enhances model performance to state-of-the-art on VSI-Bench, surpassing previous models at larger scales; we also reveal the effects of data diversity on 3D-RFT.

In summary, our key contributions are as follows:

- We propose 3D-RFT, a systematic reinforcement fine-tuning framework that extends RLVR to 3D video perception and reasoning, shifting the learning paradigm from sequence imitation to metrics-driven policy optimization.
- We design task-specific verifiable reward functions derived directly from evaluation metrics (e.g., 3D IoU, F1-Score) to enable efficient and robust policy updates.
- We conduct extensive experiments on standard video-based 3D scene understanding benchmarks, demonstrating that 3D-RFT achieves significant improvements over SFT baselines and surpasses larger-scale models in both 3D perception and reasoning tasks.

2. Related Work

MLLMs for 3D Scene Understanding. 3D perception and spatial reasoning are fundamental pillars of 3D scene understanding. Early research focused on developing unified MLLMs based on 3D sensory inputs (*e.g.*, point clouds) (Zhu et al., 2023; Xu et al., 2024; Huang et al., 2024b; Yang et al., 2024; Chen et al., 2024b; Qi et al., 2024; Zhu et al., 2024; Linghu et al., 2024; Fu et al., 2025; Chu et al., 2024; Deng et al., 2025; Mao et al., 2025). Recently, advancements in video understanding establish video-based MLLMs as a compelling approach due to the streamlined input and strong performance (El Banani et al., 2024; Man et al., 2024; Zhang et al., 2025c; Zhu et al., 2025a; Zheng et al., 2025c; Qi et al., 2025a; Huang et al., 2025b; Zhu et al., 2025b; Li et al., 2025b; Cheng et al., 2025). To bolster the 3D awareness of video-based representation, there are efforts in geometry enhancement (Wang et al., 2025a; Huang et al., 2025e; Zheng et al., 2025e; Hu et al., 2025) and data scaling (Chen et al., 2024a; Cheng et al., 2024b; Cai et al., 2025a; Ma et al., 2025b; Xu et al., 2025; Song et al., 2025; Zhang et al., 2025a; Zhou et al., 2025; Brown et al., 2025; Yang et al., 2025c; Cai et al., 2025b). However, these efforts are insufficient to resolve the persistent bottlenecks in 3D perception and spatial reasoning (Fu et al., 2024; Huang et al., 2025a; Yu et al., 2025b). In contrast, we contend that more critical issues reside in the SFT paradigm, *e.g.*, suboptimal objectives for perception tasks and overfitting issues for reasoning tasks. We address these bottlenecks through 3D-RFT, an advanced framework that demonstrates superior efficacy across 3D perception and reasoning tasks.

Reinforcement Learning for MLLMs. RLVR has catalyzed significant breakthroughs in reasoning capabilities of LLMs (Jaech et al., 2024a; Shao et al., 2024b; Guo et al., 2025; Yu et al., 2025a; Zheng et al., 2025a; Liu et al., 2025a;b; Yue et al., 2025; Wen et al., 2025) and MLLMs (Huang et al., 2025d; Team et al., 2025b; Liu et al., 2025c; Sarch et al., 2025; Tan et al., 2025). Recent efforts in video-based models have advanced Chain-of-Thought (CoT) data generation (Fei et al., 2024; Wu et al., 2024; Shao et al., 2024a; Linghu et al., 2026; Chen et al., 2025a; Zheng et al., 2025d) and employed RLVR for video understanding (Feng et al., 2025; Li et al., 2025c; Wang et al., 2025c), 3D perception (Yuan et al., 2025b; Huang et al., 2025c; Wang et al., 2025d; Ma et al., 2025a), spatial reasoning (Zhan et al., 2025; Chen et al., 2025b; Wu et al., 2025a;b), and embodied intelligence (Qi et al., 2025b; Zhao et al., 2025; Yuan et al., 2025a). However, the efficacy of RLVR for 3D scene understanding tasks is under-explored (Liao et al., 2025; Zhong et al., 2025; Yang et al., 2025b). In this work, we present a systematic study of RLVR across 3D perception and spatial reasoning tasks. Our 3D-RFT framework reveals the potential of RLVR for 3D scene understanding, highlighting key factors such as learning objective and CoT data quality.

3. Methodology

3.1. Preliminary

Reinforcement Learning with Verifiable Rewards (RLVR). RLVR has emerged as a powerful paradigm for enhancing reasoning in LLMs (Guo et al., 2025; Team et al., 2025b). Unlike SFT that maximizes the likelihood of expert data, RLVR maximizes the expected value of a verifiable outcome. Given an input prompt \mathbf{x} , the policy π_θ generates a response \mathbf{y} , which is evaluated by a deterministic verifier \mathcal{V} to yield a reward $R = \mathcal{V}(\mathbf{x}, \mathbf{y})$. The objective is to maximize the expected reward over the data distribution:

$$J(\theta) = \mathbb{E}_{\mathbf{x} \sim \mathcal{D}, \mathbf{y} \sim \pi_\theta(\cdot|\mathbf{x})}[R]. \quad (1)$$

Group Relative Policy Optimization (GRPO). GRPO (Shao et al., 2024b) is a memory-efficient variant of PPO (Schulman et al., 2017) that eliminates the need for a separate critic network. Instead of learning a value function to estimate the baseline, GRPO samples a group of outputs $\{\mathbf{y}_1, \dots, \mathbf{y}_G\}$ for each prompt \mathbf{x} from the old policy $\pi_{\theta_{old}}$. The advantage A_i for the i -th sample is then computed by normalizing its reward against the group statistics:

$$A_i = \frac{R_i - \text{mean}(\{R_1, \dots, R_G\})}{\text{std}(\{R_1, \dots, R_G\})}, \quad (2)$$

where G is the group size. This approach significantly reduces memory overhead by removing the value model.

3.2. Task Formulation

We formulate video-based 3D scene understanding as a conditional text generation problem. Given the visual input \mathbf{I} (composed of RGB video frames) and a textual query \mathbf{x} , the model generates a response sequence \mathbf{y} . To facilitate verifiable reward computation, we enforce a structured output format: the model must first generate a reasoning chain enclosed in `<think>` tags, followed by the final prediction within `<answer>` tags. We consider two perception tasks (3D video detection and 3D visual grounding) and a reasoning task (3D spatial reasoning). For 3D perception tasks, the final answer is formatted as a JSON object where 3D bounding boxes are represented as 9-DoF tuples: $\mathbf{b} = (x, y, z, w, h, d, \psi, \theta, \phi)$.

3D Video Detection. The goal is to detect all objects $\mathcal{O} = \{(\mathbf{b}_i, c_i)\}$ appearing throughout the image frames, where \mathbf{b}_i refers to the 9-DoF bounding box and c_i refers to the object category. All the bounding boxes are unified into the **coordinate system of the first frame**.

3D Visual Grounding. Given a grounding text, the model predicts a tuple $(f_{\text{pred}}, \mathbf{b}_{\text{pred}})$, identifying both the frame index and the object’s 9-DoF bounding box. Unlike detection, \mathbf{b}_{pred} is defined in the **local coordinate system of the predicted frame** f_{pred} .

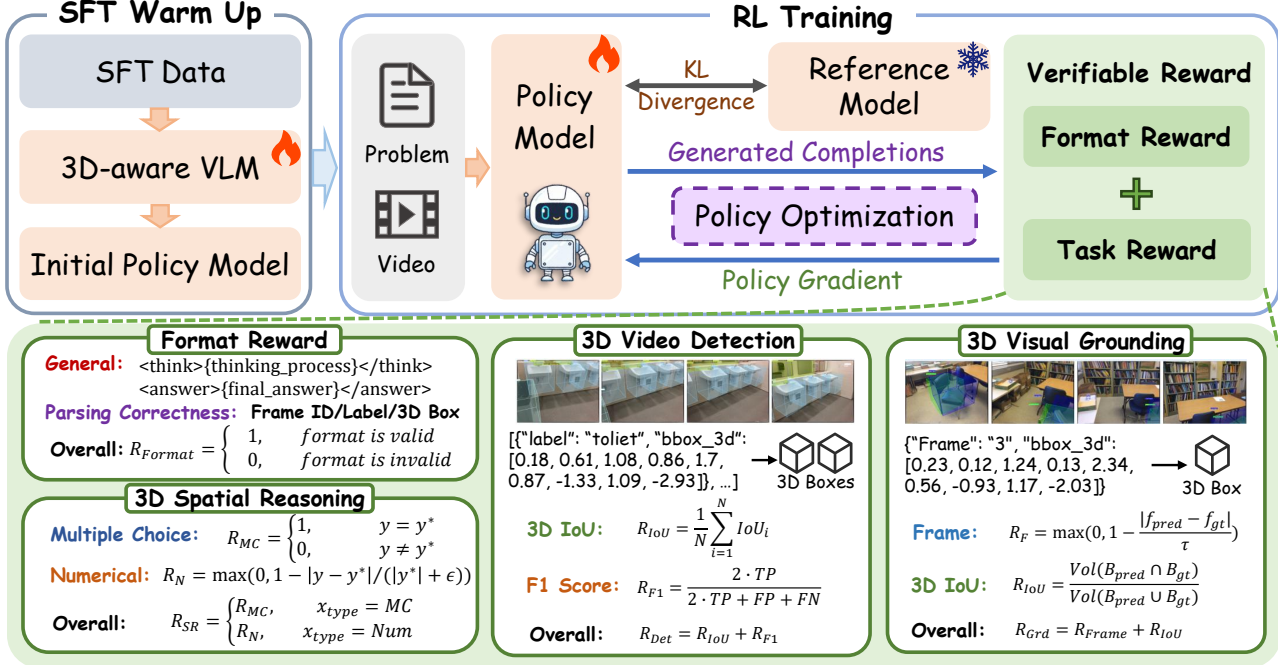


Figure 2. Overview of the 3D-RFT training framework. The process consists of two main stages: (1) **SFT Warm Up**: Initial training of the 3D-aware VLM using SFT data to establish a baseline policy. (2) **RL Training**: The Policy Model generates completions for video-based problems. A Verifiable Reward is calculated based on **Format Reward** (adherence to structured output) and **Task Reward** (performance in 3D Video Detection, 3D Visual Grounding, and Spatial Reasoning using metrics like 3D IoU and F1 Score). The model is optimized via Policy Gradient while maintaining a KL Divergence constraint relative to the frozen Reference Model.

3D Spatial Reasoning. Given a question, the model must generate accurate text answers. This task mainly focuses on spatial attributes and relations within 3D scenes.

3.3. Training Pipeline

As illustrated in Figure 2, our training pipeline consists of two stages: (1) **SFT Warm Up**, which activates the model’s capabilities of 3D scene understanding and establishes an initial policy model; and (2) **RL Training**, where the model is optimized using strictly verifiable rewards. This second stage leverages policy gradients derived from both format constraints and task-specific metrics (e.g., 3D IoU) to directly refine the model’s performance on video-based 3D scene understanding tasks.

3.3.1. STAGE 1: SFT WARM UP

Before RL training, the model must learn to follow the required output format (i.e., enclosing reasoning in `<think>` tags and presenting the final answer in proper format) and acquire basic capabilities to provide a good starting point for the subsequent RL stage. In the SFT stage, the model is trained to maximize the log-likelihood of the ground-truth response y^* given the visual input \mathbf{I} and textual query \mathbf{x} :

$$\mathcal{L}_{SFT}(\theta) = - \sum_{t=1}^T \log \pi_{\theta}(y_t^* | \mathbf{x}, \mathbf{I}, y_{<t}^*). \quad (3)$$

3.3.2. STAGE 2: RL TRAINING

In the second stage, we proceed to refine the model by employing GRPO with verifiable rewards. For each visual-textual input (\mathbf{I}, \mathbf{x}) , we sample a group of G outputs $\{y_1, \dots, y_G\}$ from the current policy $\pi_{\theta_{old}}$. The advantage A_i for each sample is computed by normalizing the rewards within the group. The objective maximizes the expected advantage while constraining the policy shift via a KL-divergence penalty with the reference model π_{ref} :

$$\mathcal{L}_{GRPO}(\theta) = - \frac{1}{\sum_{i=1}^G T_i} \sum_{i=1}^G \sum_{t=1}^{T_i} \mathcal{L}_{i,t}(\theta) + \beta \mathcal{D}_{KL}[\pi_{\theta} || \pi_{ref}], \quad (4)$$

$$\mathcal{L}_{i,t}(\theta) = \min \left(r_{i,t} A_i, \text{clip}(r_{i,t}, 1 - \epsilon, 1 + \epsilon) A_i \right), \quad (5)$$

$$r_{i,t} = \frac{\pi_{\theta}(y_{i,t} | \mathbf{I}_i, \mathbf{x}_i, y_{i,<t})}{\pi_{\theta_{old}}(y_{i,t} | \mathbf{I}_i, \mathbf{x}_i, y_{i,<t})}. \quad (6)$$

The advantage A_i is defined in Equation (2). To mitigate the high memory cost of long video contexts during training, we adopt a loss chunking technique (see details in Sec. A.2).

3.4. Verifiable Reward Design

As shown in Figure 2, our rewards include two components: a **Format Reward** to enforce structural validity (e.g., correct JSON syntax and bounding box tuples), and **Task Rewards** that directly optimize geometric and semantic metrics. We will elaborate on **Task Rewards** as follows.

3.4.1. 3D VIDEO DETECTION: 3D IOU AND F1-SCORE

In the 3D video detection task, the model outputs a set of predicted bounding boxes $\mathcal{B}_{\text{pred}} = \{\mathbf{b}_1, \dots, \mathbf{b}_N\}$. Each predicted bounding box \mathbf{b}_i is directly compared against the ground-truth labels \mathcal{B}_{gt} to derive the maximum 3D IoU \mathcal{I}_i . We adopt **Average IoU Reward** to provide a dense learning signal by averaging the maximum IoUs across all predictions:

$$R_{\text{IoU}}^{(\text{Det})} = \frac{1}{N} \sum_{i=1}^N \mathcal{I}_i. \quad (7)$$

To further enhance detection capability, we introduce the **F1-Score Reward**. A prediction is counted as a True Positive (TP) if it matches an unmatched ground-truth bounding box with a 3D IoU exceeding τ_{F1} (set to 0.25 by default); otherwise, it is treated as a False Positive (FP). Ground-truth bounding boxes that remain unmatched are regarded as False Negatives (FN). The F1-Score Reward is then computed as:

$$R_{\text{F1}} = \frac{2 \cdot \text{TP}}{2 \cdot \text{TP} + \text{FP} + \text{FN}}. \quad (8)$$

The **Average IoU Reward** ensures valid geometric precision, while the **F1-Score Reward** directly optimizes the final evaluation metric. The combined verifiable reward for 3D video detection is:

$$R_{\text{Det}} = R_{\text{IoU}}^{(\text{Det})} + R_{\text{F1}}. \quad (9)$$

3.4.2. 3D VISUAL GROUNDING: FRAME AND 3D IOU

Video-based 3D visual grounding requires spatio-temporal localization of a specific object according to the grounding text. We consider both temporal and spatial precision.

Temporal Reward. Locating the target frame index f_{gt} is formulated as a regression task. To provide a dense optimization signal, we employ a smoothed linear decay function based on the absolute temporal distance between the predicted frame index f_{pred} and the ground truth, governed by a tolerance threshold τ_{frame} (set to 5 by default):

$$R_{\text{frame}} = \max\left(0, 1 - \frac{|f_{\text{pred}} - f_{\text{gt}}|}{\tau_{\text{frame}}}\right). \quad (10)$$

IoU Reward. To align with the evaluation metric, we compute the 3D IoU in the global coordinate system. Given the predicted bounding box \mathbf{b}_{pred} in the local camera coordinates of frame f_{pred} , we first transform it to the global scene coordinates using the frame’s extrinsic matrix $M_{c \rightarrow g}^{(f_{\text{pred}})}$ and the scene’s axis-alignment matrix M_{align} : $\mathbf{b}'_{\text{pred}} = M_{\text{align}} M_{c \rightarrow g}^{(f_{\text{pred}})} \mathbf{b}_{\text{pred}}$. The IoU reward is then calculated by standard 3D IoU between the aligned prediction and the ground-truth box \mathbf{b}_{gt} :

$$R_{\text{IoU}}^{(\text{Grd})} = \frac{|\mathbf{b}'_{\text{pred}} \cap \mathbf{b}_{\text{gt}}|}{|\mathbf{b}'_{\text{pred}} \cup \mathbf{b}_{\text{gt}}|}. \quad (11)$$

The final reward for 3D visual grounding is defined as:

$$R_{\text{Grd}} = R_{\text{frame}} + R_{\text{IoU}}^{(\text{Grd})}. \quad (12)$$

3.4.3. 3D SPATIAL REASONING: ACCURACY

For the 3D spatial reasoning task, we design the accuracy reward R_{acc} by dispatching task-specific verifiers based on the question type:

- **Multiple Choice.** For multi-choice scenarios, we use an exact-match indicator function:

$$R_{\text{MC}} = \mathbb{1}(\mathbf{y} = \mathbf{y}^*) \quad (13)$$

- **Numerical Reasoning.** For numerical answers (e.g., counting), we employ the Mean Relative Accuracy (MRA) with $\mathcal{C} = \{0.50, 0.55, \dots, 0.95\}$ (Yang et al., 2025a):

$$R_{\text{num}} = \frac{1}{10} \sum_{\tau_{\text{num}} \in \mathcal{C}} \mathbb{1}\left(\frac{|\mathbf{y} - \mathbf{y}^*|}{|\mathbf{y}^*|} < 1 - \tau_{\text{num}}\right). \quad (14)$$

4. Experiments

In this section, we experiment with applying 3D-RFT to 3D perception and spatial reasoning tasks. We present the results and analyses of 3D perception tasks in Sec. 4.1, and 3D spatial reasoning task in Sec. 4.2. Additionally, we present the training dynamics of both tasks in Sec. 4.3 to visualize the model’s behaviors during 3D-RFT.

Model. We build our model 3D-RFT-4B based on VG LLM-4B (Zheng et al., 2025b), which consists of an MLLM backbone, Qwen2.5-VL-3B-Instruct (Bai et al., 2025b), and a visual geometry backbone VGGT-1B (Wang et al., 2025b). Features extracted from the VGGT backbone are first processed to align with the Qwen visual feature structure, and then combined via element-wise addition, producing a hybrid visual representation that is fed into the Qwen LLM.

4.1. 3D Perception Tasks

Training Datasets. For 3D perception tasks, we follow the settings of VG LLM (Zheng et al., 2025b), utilizing ScanRefer (Chen et al., 2020), Scan2Cap (Chen et al., 2021), and ScanNetDetection (Wang et al., 2024) for the SFT stage. We have not included CoT data in this stage due to the difficulty of acquiring high-quality data. In the second stage, we conduct Reinforcement Fine-Tuning (RFT) using ScanNetDetection and ScanRefer for 3D video detection and 3D visual grounding, respectively. We provide a detailed description of the data in Sec. A.1.

Comparison Baselines and Evaluation Metrics. For 3D perception tasks, we mainly compare our model (i.e., 3D-RFT-4B) with VG LLM (Zheng et al., 2025b) to demonstrate the effectiveness of 3D-RFT. Our evaluation metrics

Table 1. **Quantitative results on ScanNetDetection.** In this table, we present the comparison with baseline models and report the performance improvement between the SFT baseline (VG LLM-4B) and 3D-RFT-4B (ours).

Model	chair	cabinet	table	bin	couch	bed	bathtub	toilet	20 Common Classes		
									P_{25}	R_{25}	$F1_{25}$
<i>4-Frame Setting</i>											
Qwen2.5-VL-3B (Zheng et al., 2025b)	37.7	10.2	35.0	23.1	39.0	64.8	32.4	68.8	32.6	27.9	30.0
Qwen2.5-VL-7B (Zheng et al., 2025b)	41.2	11.6	36.5	30.2	41.1	68.2	36.6	68.7	34.6	31.0	32.5
VG LLM-4B (Zheng et al., 2025b)	49.7	13.1	41.3	39.2	44.6	71.2	33.5	83.4	41.7	35.7	38.2
VG LLM-8B (Zheng et al., 2025b)	54.0	17.1	46.5	39.8	47.0	74.1	42.1	82.5	43.4	39.6	41.2
3D-RFT-4B (ours)	55.3	18.7	48.2	39.1	49.8	77.1	50.0	86.1	54.2	38.2	43.7
<i>Improvement</i>	+5.6	+5.6	+6.9	-0.1	+5.2	+5.9	+16.5	+2.7	+12.5	+2.5	+5.5
<i>6-Frame Setting</i>											
Qwen2.5-VL-3B (Zheng et al., 2025b)	32.8	7.8	31.3	20.9	32.2	58.8	36.5	66.1	27.8	24.1	25.7
Qwen2.5-VL-7B (Zheng et al., 2025b)	36.1	10.6	32.7	25.0	40.7	64.6	38.4	68.6	31.8	28.0	29.6
VG LLM-4B (Zheng et al., 2025b)	41.6	12.4	39.8	33.1	45.0	70.2	33.8	80.6	39.7	34.0	36.4
VG LLM-8B (Zheng et al., 2025b)	48.7	17.9	44.8	38.5	46.4	75.8	40.4	83.2	43.5	38.7	40.8
3D-RFT-4B (ours)	49.2	18.5	44.9	34.6	48.3	74.1	51.4	81.1	53.4	35.7	41.7
<i>Improvement</i>	+7.6	+6.1	+5.1	+1.5	+3.3	+3.9	+17.6	+0.5	+13.7	+1.7	+5.3

Table 2. **Quantitative results on ScanRefer.** The content in “()” indicates results with proposal refinement (Zheng et al., 2025b).

Model	3D Scene Input	Acc@0.25	Acc@0.5
ScanRefer (Chen et al., 2020)	✓	37.3	24.3
MVT (Huang et al., 2022b)	✓	40.8	33.3
ViL3DRel (Chen et al., 2022)	✓	47.9	37.7
3D-LLM (Chen et al., 2024c)	✓	30.3	-
Chat-3D v2 (Huang et al., 2024a)	✓	35.9	30.4
Grounded 3D-LLM (Chen et al., 2024c)	✓	47.9	44.1
ChatScene (Huang et al., 2024a)	✓	55.5	50.2
LLaVA-3D (Zhu et al., 2025a)	✓	54.1	42.4
Video-3D LLM (Zheng et al., 2025c)	✓	58.1	51.7
SPAR (Zhang et al., 2025a)	✗	31.9 (48.8)	12.4 (43.1)
VG LLM-4B (Zheng et al., 2025b)	✗	36.4 (53.5)	11.8 (47.5)
VG LLM-8B (Zheng et al., 2025b)	✗	41.6 (57.6)	14.9 (50.9)
3D-RFT-4B (ours)	✗	42.9 (54.6)	15.9 (48.1)
<i>Improvement</i>	✗	+6.5 (+1.1)	+4.1 (+0.6)

follow VG LLM: for ScanRefer, we report the accuracy at IoU thresholds of 0.25 and 0.5; for ScanNetDetection, we report precision, recall, and F1-score for 20 common object classes at an IoU threshold of 0.25. We use `lmms_eval` (Zhang et al., 2025b) for evaluation and keep the same evaluation hyper-parameters as VG LLM.

Results. We report the detailed evaluation results of 3D video detection and 3D visual grounding in Tabs. 1 and 2, respectively. The results show that 3D-RFT-4B achieves state-of-the-art performances on 3D perception tasks. We provide further interpretations and analyses as follows.

4.1.1. 3D VIDEO DETECTION

3D-RFT significantly enhances detection performance over the SFT baseline. As detailed in Tab. 1, 3D-RFT-4B achieves substantial gains across all metrics. Under the *4-frame setting*, our method improves Precision by +12.5%, Recall by +2.5%, and F1-Score by +5.5% compared to the SFT baseline (VG LLM-4B). The improvements are robust across settings, with the *6-frame setting* yielding even higher gains in Precision (+13.7%) and comparable boosts in F1

Table 3. **Ablation study of training strategies and 3D priors.** We report accuracy at IoU thresholds 0.25 and 0.5.

Training Strategy	3D Prior	ScanRefer	
		Acc@0.25	Acc@0.5
SFT	None	31.9 (49.9)	9.3 (43.8)
SFT → SFT	None	34.2 (50.6)	10.4 (44.9)
SFT → RL	None	38.2 (52.7)	12.1 (46.6)
SFT	VGGT	36.4 (53.5)	11.8 (47.5)
SFT → RL	VGGT	42.9 (54.6)	15.9 (48.1)

(+5.3%). Notably, the improvements are most pronounced for larger objects, such as “bathtub” (+16.5%) and “table” (+6.9%), whereas smaller objects like “bin” show more limited gains, suggesting that further increases in visual resolution could potentially benefit small-object detection.

3D-RFT-4B surpasses the larger VG LLM-8B model. With only half the parameters, 3D-RFT-4B consistently outperforms VG LLM-8B on F1-Score and Precision for both *4-frame* and *6-frame* settings. Our model also achieves superior per-class performance on the majority of object categories. This demonstrates that 3D-RFT’s metrics-driven optimization exploits the model’s potential far more effectively than the standard SFT, enabling a 4B model to exceed the capabilities of an 8B baseline.

4.1.2. 3D VISUAL GROUNDING

3D-RFT significantly enhances performance compared to the SFT baseline. As shown in Tab. 2, 3D-RFT-4B achieves substantial gains over the VG LLM-4B baseline, elevating the Acc@IoU0.25 and Acc@IoU0.5 by +6.5% and +4.5% respectively. This performance leap confirms that the RFT stage effectively refines the policy’s spatio-temporal grounding capabilities.

3D-RFT-4B outperforms the larger VG LLM-8B. With

Table 4. Quantitative results on VSI-Bench. We include zero-shot results of base models, and test results of models after SFT and RFT.

Model	Avg.	Numerical Answer				Multiple-Choice Answer			
		Obj. Count	Abs. Dist.	Obj. Size	Room Size	Rel. Dist.	Rel. Dir.	Route Plan	Appr. Order
<i>Base Models</i>									
GPT-4o (Hurst et al., 2024)	34.0	46.2	5.3	43.8	38.2	37.0	41.3	31.5	28.5
Gemini-2.5 Pro (Comanici et al., 2025)	51.5	43.8	34.9	64.3	42.8	61.1	47.8	45.9	71.3
LLaVA-Video-7B (Zhang et al., 2025c)	35.6	48.5	14.0	47.8	24.2	43.5	42.4	34.0	30.6
Qwen2.5-VL-7B (Bai et al., 2025b)	32.7	34.5	19.4	47.6	40.8	32.8	24.5	32.5	29.4
InternVL3-8B (Zhu et al., 2025c)	42.1	68.1	39.0	48.4	33.6	48.3	36.4	27.3	35.4
<i>Supervised Fine-Tuned</i>									
VG LLM-4B (Zheng et al., 2025b)	47.3	66.0	37.8	55.2	59.2	44.6	45.6	33.5	36.4
VLM-3R-7B (Fan et al., 2025)	60.9	70.2	49.4	69.2	67.1	65.4	80.5	45.4	40.1
Cambrian-S-3B (Yang et al., 2025c)	57.3	70.7	40.6	68.0	46.3	64.8	61.9	27.3	78.8
VST-SFT-3B (Yang et al., 2025b)	57.9	69.3	45.4	71.8	62.4	59.0	46.0	38.7	70.2
<i>Reinforcement Fine-Tuned</i>									
vsGRPO-2B (Liao et al., 2025)	35.4	53.6	29.0	52.7	43.4	28.1	30.9	26.8	18.9
vsGRPO-7B (Liao et al., 2025)	40.7	59.9	29.6	50.8	48.3	35.4	35.6	34.0	31.5
SpaceR-7B (Ouyang et al., 2025)	43.5	61.9	28.6	60.9	35.2	38.2	46.0	31.4	45.6
Spatial-MLLM-4B (Wu et al., 2025a)	48.4	65.3	34.8	63.1	45.1	41.3	46.2	33.5	46.3
ViLaSR-7B (Wu et al., 2025b)	45.4	63.5	34.4	60.6	30.9	48.9	45.2	30.4	49.2
SpatialLadder-3B (Li et al., 2025a)	45.7	63.5	34.3	61.7	43.9	45.4	44.8	35.6	36.4
VST-RL-3B (Yang et al., 2025b)	57.7	66.6	45.0	72.8	60.9	59.9	47.6	40.7	68.3
3D-RFT-4B (ours)	62.8	71.2	53.5	70.3	63.2	60.8	77.9	37.6	67.8

only half the parameters, 3D-RFT-4B surpasses VG LLM-8B (42.9% vs. 41.6% on Acc@IoU0.25). We attribute the advantage to the learning objective: while SFT focuses on maximizing the likelihood of ground-truth labels, 3D-RFT directly optimizes towards more geometrically precise grounding results. This effectively drives the model to learn tighter and more accurate bounding boxes, which is unlikely to emerge from the imitation learning of SFT.

4.1.3. ANALYSIS OF RFT AND 3D PRIOR

The efficacy of RFT is robust across diverse visual inputs.

We further ablate the VGGT input to investigate whether the efficacy of 3D-RFT is consistent: (1) vanilla Qwen2.5-VL (No 3D Prior), and (2) Qwen2.5-VL augmented with VGGT. The results demonstrate consistent improvements under both settings, with the VGGT-equipped model improving from 36.4% to 42.9% on Acc@0.25 after RFT. This confirms that 3D-RFT consistently enhances the model’s capability regardless of visual inputs, e.g., the presence of 3D priors.

4.2. 3D Spatial Reasoning

Formulation. We consider two settings for the spatial reasoning task: (1) Direct-Answer (DA), where the model is prompted to directly output the final answer; and (2) Think-Answer (TA), where the model is prompted to think before giving the final answer. In this task, we conduct RFT in the TA setting following common practices, and experiment with two schemes for the SFT stage: (1) default SFT (DA+TA), where we use both DA and TA data; and (2) SFT (DA), where we exclude TA data (i.e., CoT data).

Training Data. We curate a data mixture from VLM-3R (Fan et al., 2025) and SpaceR (Ouyang et al., 2025), in-

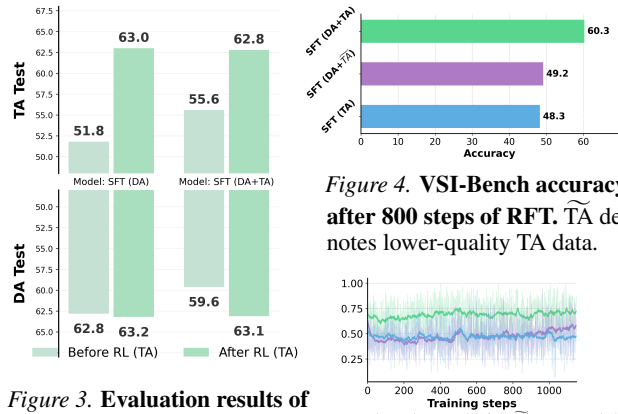


Figure 3. Evaluation results of SFT and RFT on VSI-Bench. The results include comparison of SFT checkpoints, RFT efficacy, and TA/DA test settings.

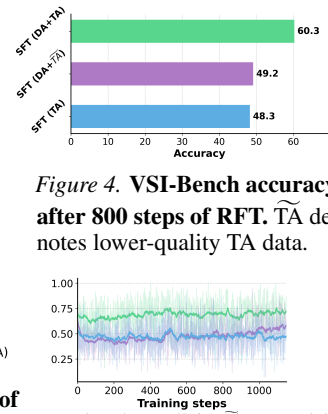


Figure 4. VSI-Bench accuracy after 800 steps of RFT. $\tilde{\text{TA}}$ denotes lower-quality TA data.

Figure 5. Accuracy rewards during RFT. $\tilde{\text{TA}}$ denotes lower-quality TA data.

cluding 298K data instances in total, termed VSI-298K. Additionally, we generate 10K high-quality CoT data using Qwen3-VL-32B-Thinking (Bai et al., 2025a), termed CoT-10K. By default, we use the mixture of VSI-298K (DA) and CoT-10K (TA) for SFT, and VSI-298K for RFT (TA).

Results. We present the evaluation results on VSI-Bench in Tab. 4. The results show that 3D-RFT-4B outperforms prior methods by a large margin, especially on numerical reasoning categories. This suggests that RFT provides more effective learning signals compared to SFT. We will present further analyses on RFT efficacy and data as follows.

4.2.1. ANALYSIS OF RFT AND DATA

3D-RFT consistently improves spatial reasoning performance. As shown in Fig. 3, we present evaluation results

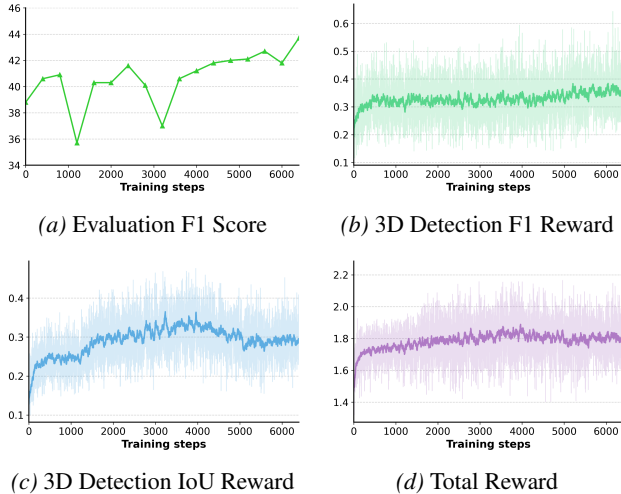


Figure 6. Training Dynamics Analysis (3D Video Detection).

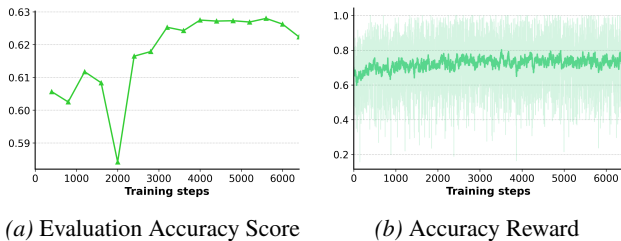


Figure 7. Training Dynamics Analysis (3D Spatial Reasoning).

regarding two SFT checkpoints, and compare their performances between “before” and “after” RFT. The results demonstrate that RFT yields consistent improvements on VSI-Bench, especially on TA test. Moreover, RFT on TA task elicits improvements on DA task. In addition, we observe that continually training with SFT yields a moderate performance drop, which suggests the advantage of RFT.

DA data and TA data shape the foundation of RFT. We compare the RFT results given different SFT data schemes: (1) default SFT (DA+TA); (2) SFT (DA+ \tilde{TA}), where we replace the CoT-10K data with 10K lower-quality CoT data generated by Qwen2.5-VL-72B-Instruct (Bai et al., 2025b); and (3) SFT (DA), which only uses CoT-10K during SFT. We compare their evaluation results and training rewards in Fig. 5. The results show that the SFT (DA+TA) exhibits consistently higher accuracy and rewards than SFT (DA+ \tilde{TA}) and SFT (TA). This suggests that the foundation of RFT relies on both DA data that teaches In-Domain (ID) knowledge and high-quality TA data (*i.e.*, CoT data) that teaches accurate reasoning behaviors.

TA data prevents overfitting and ensures reliable reasoning behavior. While SFT (DA) exhibits competitive In-Domain (ID) performance on VSI-Bench (Fig. 3), we observe it shows significantly poorer Out-Of-Domain (OOD) performance than SFT (DA+TA) (Sec. C.1). On the other

hand, we observe that SFT (DA) can emerge reasoning output format, but the thoughts could be unreliable, *e.g.*, tedious text like R1-Zero (Guo et al., 2025). This suggests that TA data is critical for generalization and reliable reasoning behavior, and we should avoid training MLLMs solely on DA data.

4.3. Training Dynamics

3D Video Detection. Fig. 6 illustrates the training dynamics of 3D-RFT on 3D video detection. The consistent rise in both Evaluation F1 Score (a) and F1 Reward (b) confirms that RFT effectively optimizes perception. Analyzing the reward components reveals a strategic shift: while the global F1 Reward (b) steadily increases, the IoU Reward (c) peaks early and then slightly declines. This indicates the policy transitions from initial *geometric refinement* (tightening boxes) to *recall maximization* (reducing false negatives). In the latter phase, the dense IoU Reward serves as a critical regulator, while the sparser F1 Reward optimizes the global balance between precision and recall. Moreover, the continuous improvement at the end implies that RLVR is a stable and effective paradigm for 3D perception tasks.

3D Spatial Reasoning. Fig. 7 illustrates the training dynamics of 3D-RFT on the spatial reasoning task. Despite minor fluctuations, both evaluation accuracy and training rewards exhibit upward trends, confirming RFT’s efficacy. Notably, the curves show a sign of saturation after 4000 steps. We attribute this to the nature of the optimization landscape: unlike perception tasks where RFT continuously refines continuous geometric coordinates, the reasoning task features a discrete text space with coarser feedback. This leads to the earlier saturation than 3D perception tasks, and potentially limits the granularity of improvement over SFT.

5. Conclusion

We introduce 3D-RFT, a framework that applies RLVR to video-based 3D scene understanding. By shifting the learning paradigm from token-level imitation to direct metrics-driven optimization, *i.e.*, utilizing verifiable rewards like 3D IoU and F1-Score, 3D-RFT effectively aligns training objectives with task performance. We demonstrate that 3D-RFT effectively enhances model performance across perception tasks and reasoning tasks, including 3D video detection, 3D visual grounding, and spatial reasoning. Our model 3D-RFT-4B even outperforms larger baselines like VG LLM-8B in 3D video detection and VLM-3R-7B in spatial reasoning. Our analyses reveal good properties of 3D-RFT such as robust efficacy, and valuable insights like the impact of data diversity. We hope our work can unveil the potential of RLVR for 3D scene understanding and offer valuable insights for future research.

Impact Statement

This paper presents work whose goal is to advance the field of Machine Learning. There are many potential societal consequences of our work, none of which we feel must be specifically highlighted here.

References

- Bai, S., Cai, Y., Chen, R., Chen, K., Chen, X., Cheng, Z., Deng, L., Ding, W., Gao, C., Ge, C., Ge, W., Guo, Z., Huang, Q., Huang, J., Huang, F., Hui, B., Jiang, S., Li, Z., Li, M., Li, M., Li, K., Lin, Z., Lin, J., Liu, X., Liu, J., Liu, C., Liu, Y., Liu, D., Liu, S., Lu, D., Luo, R., Lv, C., Men, R., Meng, L., Ren, X., Ren, X., Song, S., Sun, Y., Tang, J., Tu, J., Wan, J., Wang, P., Wang, P., Wang, Q., Wang, Y., Xie, T., Xu, Y., Xu, H., Xu, J., Yang, Z., Yang, M., Yang, J., Yang, A., Yu, B., Zhang, F., Zhang, H., Zhang, X., Zheng, B., Zhong, H., Zhou, J., Zhou, F., Zhou, J., Zhu, Y., and Zhu, K. Qwen3-vl technical report. *arXiv preprint arXiv:2511.21631*, 2025a.
- Bai, S., Chen, K., Liu, X., Wang, J., Ge, W., Song, S., Dang, K., Wang, P., Wang, S., Tang, J., Zhong, H., Zhu, Y., Yang, M., Li, Z., Wan, J., Wang, P., Ding, W., Fu, Z., Xu, Y., Ye, J., Zhang, X., Xie, T., Cheng, Z., Zhang, H., Yang, Z., Xu, H., and Lin, J. Qwen2.5-vl technical report. *arXiv preprint arXiv:2502.13923*, 2025b.
- Baruch, G., Chen, Z., Dehghan, A., Dimry, T., Feigin, Y., Fu, P., Gebauer, T., Joffe, B., Kurz, D., Schwartz, A., et al. Arkitscenes: A diverse real-world dataset for 3d indoor scene understanding using mobile rgb-d data. In *Advances in Neural Information Processing Systems (NeurIPS)*, 2021.
- Brohan, A., Brown, N., Carbajal, J., Chebotar, Y., Chen, X., Chormanski, K., Ding, T., Driess, D., Dubey, A., Finn, C., et al. Rt-2: Vision-language-action models transfer web knowledge to robotic control. In *Conference on Robot Learning (CoRL)*, 2023.
- Brown, E., Ray, A., Krishna, R., Girshick, R., Ferguson, R., and Xie, S. Sims-v: Simulated instruction-tuning for spatial video understanding. *arXiv preprint arXiv:2511.04668*, 2025.
- Cai, W., Ponomarenko, I., Yuan, J., Li, X., Yang, W., Dong, H., and Zhao, B. Spatialbot: Precise spatial understanding with vision language models. In *International Conference on Robotics and Automation (ICRA)*, 2025a.
- Cai, Z., Wang, R., Gu, C., Pu, F., Xu, J., Wang, Y., Yin, W., Yang, Z., Wei, C., Sun, Q., et al. Scaling spatial intelligence with multimodal foundation models. *arXiv preprint arXiv:2511.13719*, 2025b.
- Chen, B., Xu, Z., Kirmani, S., Ichter, B., Sadigh, D., Guibas, L., and Xia, F. Spatialvlm: Endowing vision-language models with spatial reasoning capabilities. In *Conference on Computer Vision and Pattern Recognition (CVPR)*, 2024a.
- Chen, D. Z., Chang, A. X., and Nießner, M. Scanrefer: 3d object localization in rgb-d scans using natural language. In *European Conference on Computer Vision (ECCV)*, 2020.
- Chen, S., Guhur, P.-L., Tapaswi, M., Schmid, C., and Laptev, I. Language conditioned spatial relation reasoning for 3d object grounding. In *Advances in Neural Information Processing Systems (NeurIPS)*, 2022.
- Chen, S., Chen, X., Zhang, C., Li, M., Yu, G., Fei, H., Zhu, H., Fan, J., and Chen, T. Ll3da: Visual interactive instruction tuning for omni-3d understanding, reasoning, and planning. In *Conference on Computer Vision and Pattern Recognition (CVPR)*, 2024b.
- Chen, Y., Yang, S., Huang, H., Wang, T., Xu, R., Lyu, R., Lin, D., and Pang, J. Grounded 3d-llm with referent tokens. *arXiv preprint arXiv:2405.10370*, 2024c.
- Chen, Y., Qi, Z., Zhang, W., Jin, X., Zhang, L., and Liu, P. Reasoning in space via grounding in the world. *arXiv preprint arXiv:2510.13800*, 2025a.
- Chen, Z., Gholami, A., Nießner, M., and Chang, A. X. Scan2cap: Context-aware dense captioning in rgb-d scans. In *Conference on Computer Vision and Pattern Recognition (CVPR)*, 2021.
- Chen, Z., Zhang, M., Yu, X., Luo, X., Sun, M., Pan, Z., Feng, Y., Pei, P., Cai, X., and Huang, R. Think with 3d: Geometric imagination grounded spatial reasoning from limited views. *arXiv preprint arXiv:2510.18632*, 2025b.
- Cheng, A.-C., Ji, Y., Yang, Z., Gongye, Z., Zou, X., Kautz, J., Bıyık, E., Yin, H., Liu, S., and Wang, X. Navila: Legged robot vision-language-action model for navigation. *arXiv preprint arXiv:2412.04453*, 2024a.
- Cheng, A.-C., Yin, H., Fu, Y., Guo, Q., Yang, R., Kautz, J., Wang, X., and Liu, S. Spatialrgpt: Grounded spatial reasoning in vision-language models. In *Advances in Neural Information Processing Systems (NeurIPS)*, 2024b.
- Cheng, A.-C., Fu, Y., Chen, Y., Liu, Z., Li, X., Radhakrishnan, S., Han, S., Lu, Y., Kautz, J., Molchanov, P., et al. 3d aware region prompted vision language model. *arXiv preprint arXiv:2509.13317*, 2025.
- Chu, T., Zhang, P., Dong, X., Zang, Y., Liu, Q., and Wang, J. Unified scene representation and reconstruction for 3d large language models. *arXiv preprint arXiv:2404.13044*, 2024.

- Comanici, G., Bieber, E., Schaekermann, M., Pasupat, I., Sachdeva, N., Dhillon, I., Blistein, M., Ram, O., Zhang, D., Rosen, E., et al. Gemini 2.5: Pushing the frontier with advanced reasoning, multimodality, long context, and next generation agentic capabilities. *arXiv preprint arXiv:2507.06261*, 2025.
- Dai, A., Chang, A. X., Savva, M., Halber, M., Funkhouser, T., and Nießner, M. Scannet: Richly-annotated 3d reconstructions of indoor scenes. In *Conference on Computer Vision and Pattern Recognition (CVPR)*, 2017.
- Deng, J., He, T., Jiang, L., Wang, T., Dayoub, F., and Reid, I. 3d-llava: Towards generalist 3d llms with omni superpoint transformer. In *Conference on Computer Vision and Pattern Recognition (CVPR)*, 2025.
- Driess, D., Xia, F., Sajjadi, M. S., Lynch, C., Chowdhery, A., Ichter, B., Wahid, A., Tompson, J., Vuong, Q., Yu, T., et al. Palm-e: An embodied multimodal language model. In *International Conference on Machine Learning (ICML)*, 2023.
- El Banani, M., Raj, A., Maninis, K.-K., Kar, A., Li, Y., Rubinstein, M., Sun, D., Guibas, L., Johnson, J., and Jampani, V. Probing the 3d awareness of visual foundation models. In *Conference on Computer Vision and Pattern Recognition (CVPR)*, 2024.
- Fan, Z., Zhang, J., Li, R., Zhang, J., Chen, R., Hu, H., Wang, K., Qu, H., Wang, D., Yan, Z., et al. Vlm-3r: Vision-language models augmented with instruction-aligned 3d reconstruction. *arXiv preprint arXiv:2505.20279*, 2025.
- Fei, H., Wu, S., Ji, W., Zhang, H., Zhang, M., Lee, M. L., and Hsu, W. Video-of-thought: step-by-step video reasoning from perception to cognition. In *International Conference on Machine Learning (ICML)*, 2024.
- Feng, K., Gong, K., Li, B., Guo, Z., Wang, Y., Peng, T., Wu, J., Zhang, X., Wang, B., and Yue, X. Video-r1: Reinforcing video reasoning in mllms. In *Advances in Neural Information Processing Systems (NeurIPS)*, 2025.
- Fu, R., Liu, J., Chen, X., Nie, Y., and Xiong, W. Scene-llm: Extending language model for 3d visual understanding and reasoning. In *Proceedings of Winter Conference on Applications of Computer Vision (WACV)*, 2025.
- Fu, X., Hu, Y., Li, B., Feng, Y., Wang, H., Lin, X., Roth, D., Smith, N. A., Ma, W.-C., and Krishna, R. Blink: Multimodal large language models can see but not perceive. In *European Conference on Computer Vision (ECCV)*, 2024.
- Gong, R., Huang, J., Zhao, Y., Geng, H., Gao, X., Wu, Q., Ai, W., Zhou, Z., Terzopoulos, D., Zhu, S.-C., et al. Arnold: A benchmark for language-grounded task learning with continuous states in realistic 3d scenes. In *International Conference on Computer Vision (ICCV)*, 2023.
- Guo, D., Yang, D., Zhang, H., Song, J., Zhang, R., Xu, R., Zhu, Q., Ma, S., Wang, P., Bi, X., et al. Deepseek-r1: Incentivizing reasoning capability in llms via reinforcement learning. *arXiv preprint arXiv:2501.12948*, 2025.
- Hu, E. J., Shen, Y., Wallis, P., Allen-Zhu, Z., Li, Y., Wang, S., Wang, L., and Chen, W. Lora: Low-rank adaptation of large language models. In *International Conference on Learning Representations (ICLR)*, 2022.
- Hu, W., Lin, J., Long, Y., Ran, Y., Jiang, L., Wang, Y., Zhu, C., Xu, R., Wang, T., and Pang, J. G²vlm: Geometry grounded vision language model with unified 3d reconstruction and spatial reasoning. *arXiv preprint arXiv:2511.21688*, 2025.
- Huang, H., Chen, Y., Wang, Z., Huang, R., Xu, R., Wang, T., Liu, L., Cheng, X., Zhao, Y., Pang, J., et al. Chat-scene: Bridging 3d scene and large language models with object identifiers. In *Advances in Neural Information Processing Systems (NeurIPS)*, 2024a.
- Huang, J., Zhu, W. Y., Jia, B., Wang, Z., Ma, X., Li, Q., and Huang, S. Perceive, ground, reason, and act: A benchmark for general-purpose visual representation. *arXiv preprint arXiv:2211.15402*, 2022a.
- Huang, J., Yong, S., Ma, X., Linghu, X., Li, P., Wang, Y., Li, Q., Zhu, S.-C., Jia, B., and Huang, S. An embodied generalist agent in 3d world. In *International Conference on Machine Learning (ICML)*, 2024b.
- Huang, J., Jia, B., Wang, Y., Zhu, Z., Linghu, X., Li, Q., Zhu, S.-C., and Huang, S. Unveiling the mist over 3d vision-language understanding: Object-centric evaluation with chain-of-analysis. In *Conference on Computer Vision and Pattern Recognition (CVPR)*, 2025a.
- Huang, J., Ma, X., Linghu, X., Fan, Y., He, J., Tan, W., Li, Q., Zhu, S.-C., Chen, Y., Jia, B., et al. Leo-vl: Efficient scene representation for scalable 3d vision-language learning. *arXiv preprint arXiv:2506.09935*, 2025b.
- Huang, S., Chen, Y., Jia, J., and Wang, L. Multi-view transformer for 3d visual grounding. In *Conference on Computer Vision and Pattern Recognition (CVPR)*, 2022b.
- Huang, T., Zhang, Z., and Tang, H. 3d-r1: Enhancing reasoning in 3d vlms for unified scene understanding. *arXiv preprint arXiv:2507.23478*, 2025c.
- Huang, W., Jia, B., Zhai, Z., Cao, S., Ye, Z., Zhao, F., Xu, Z., Hu, Y., and Lin, S. Vision-r1: Incentivizing reasoning capability in multimodal large language models. *arXiv preprint arXiv:2503.06749*, 2025d.

- Huang, X., Wu, J., Xie, Q., and Han, K. Mllms need 3d-aware representation supervision for scene understanding. In *Advances in Neural Information Processing Systems (NeurIPS)*, 2025e.
- Hurst, A., Lerer, A., Goucher, A. P., Perelman, A., Ramesh, A., Clark, A., Ostrow, A., Welihinda, A., Hayes, A., Radford, A., et al. Gpt-4o system card. *arXiv preprint arXiv:2410.21276*, 2024.
- Jaech, A., Kalai, A., Lerer, A., Richardson, A., El-Kishky, A., Low, A., Helyar, A., Madry, A., Beutel, A., Carney, A., et al. Openai o1 system card. *arXiv preprint arXiv:2412.16720*, 2024a.
- Jaech, A., Kalai, A., Lerer, A., Richardson, A., El-Kishky, A., Low, A., Helyar, A., Madry, A., Beutel, A., Carney, A., et al. Openai o1 system card. *arXiv preprint arXiv:2412.16720*, 2024b.
- Li, H., Li, D., Wang, Z., Yan, Y., Wu, H., Zhang, W., Shen, Y., Lu, W., Xiao, J., and Zhuang, Y. Spatialladder: Progressive training for spatial reasoning in vision-language models. *arXiv preprint arXiv:2510.08531*, 2025a.
- Li, R., Li, S., Kong, L., Yang, X., and Liang, J. Seeground: See and ground for zero-shot open-vocabulary 3d visual grounding. In *Conference on Computer Vision and Pattern Recognition (CVPR)*, 2025b.
- Li, X., Yan, Z., Meng, D., Dong, L., Zeng, X., He, Y., Wang, Y., Qiao, Y., Wang, Y., and Wang, L. Videochat-r1: Enhancing spatio-temporal perception via reinforcement fine-tuning. *arXiv preprint arXiv:2504.06958*, 2025c.
- Liao, Z., Xie, Q., Zhang, Y., Kong, Z., Lu, H., Yang, Z., and Deng, Z. Improved visual-spatial reasoning via r1-zero-like training. *arXiv preprint arXiv:2504.00883*, 2025.
- Linghu, X., Huang, J., Niu, X., Ma, X. S., Jia, B., and Huang, S. Multi-modal situated reasoning in 3d scenes. In *Advances in Neural Information Processing Systems (NeurIPS)*, 2024.
- Linghu, X., Huang, J., Zhu, Z., Jia, B., and Huang, S. Scenecot: Eliciting grounded chain-of-thought reasoning in 3d scenes. In *International Conference on Learning Representations (ICLR)*, 2026.
- Liu, H., Li, C., Wu, Q., and Lee, Y. J. Visual instruction tuning. In *Advances in Neural Information Processing Systems (NeurIPS)*, 2023.
- Liu, Z., Chen, C., Li, W., Qi, P., Pang, T., Du, C., Lee, W. S., and Lin, M. Understanding r1-zero-like training: A critical perspective. In *Conference on Language Modeling (COLM)*, 2025a.
- Liu, Z., Liu, J., He, Y., Wang, W., Liu, J., Pan, L., Hu, X., Xiong, S., Huang, J., Hu, J., et al. Part i: Tricks or traps? a deep dive into rl for llm reasoning. *arXiv preprint arXiv:2508.08221*, 2025b.
- Liu, Z., Sun, Z., Zang, Y., Dong, X., Cao, Y., Duan, H., Lin, D., and Wang, J. Visual-rft: Visual reinforcement fine-tuning. In *International Conference on Computer Vision (ICCV)*, 2025c.
- Ma, W., Chou, Y.-C., Liu, Q., Wang, X., de Melo, C., Xie, J., and Yuille, A. Spatialreasoner: Towards explicit and generalizable 3d spatial reasoning. In *Advances in Neural Information Processing Systems (NeurIPS)*, 2025a.
- Ma, W., Ye, L., de Melo, C. M., Yuille, A., and Chen, J. Spatialllm: A compound 3d-informed design towards spatially-intelligent large multimodal models. In *Conference on Computer Vision and Pattern Recognition (CVPR)*, 2025b.
- Ma, X., Yong, S., Zheng, Z., Li, Q., Liang, Y., Zhu, S.-C., and Huang, S. Sqa3d: Situated question answering in 3d scenes. In *International Conference on Learning Representations (ICLR)*, 2023.
- Man, Y., Zheng, S., Bao, Z., Hebert, M., Gui, L.-Y., and Wang, Y.-X. Lexicon3d: Probing visual foundation models for complex 3d scene understanding. *Advances in Neural Information Processing Systems (NeurIPS)*, 2024.
- Mao, Y., Zhong, J., Fang, C., Zheng, J., Tang, R., Zhu, H., Tan, P., and Zhou, Z. Spatialllm: Training large language models for structured indoor modeling. In *Advances in Neural Information Processing Systems (NeurIPS)*, 2025.
- Ouyang, K., Liu, Y., Wu, H., Liu, Y., Zhou, H., Zhou, J., Meng, F., and Sun, X. Spacer: Reinforcing mllms in video spatial reasoning. *arXiv preprint arXiv:2504.01805*, 2025.
- Qi, Z., Fang, Y., Sun, Z., Wu, X., Wu, T., Wang, J., Lin, D., and Zhao, H. Gpt4point: A unified framework for point-language understanding and generation. In *Conference on Computer Vision and Pattern Recognition (CVPR)*, 2024.
- Qi, Z., Zhang, Z., Fang, Y., Wang, J., and Zhao, H. Gpt4scene: Understand 3d scenes from videos with vision-language models. *arXiv preprint arXiv:2501.01428*, 2025a.
- Qi, Z., Zhang, Z., Yu, Y., Wang, J., and Zhao, H. Vln-r1: Vision-language navigation via reinforcement fine-tuning. *arXiv preprint arXiv:2506.17221*, 2025b.
- Sarch, G., Saha, S., Khandelwal, N., Jain, A., Tarr, M. J., Kumar, A., and Fragkiadaki, K. Grounded reinforcement

- learning for visual reasoning. In *Advances in Neural Information Processing Systems (NeurIPS)*, 2025.
- Schulman, J., Wolski, F., Dhariwal, P., Radford, A., and Klimov, O. Proximal policy optimization algorithms. *arXiv preprint arXiv:1707.06347*, 2017.
- Shao, H., Qian, S., Xiao, H., Song, G., Zong, Z., Wang, L., Liu, Y., and Li, H. Visual cot: Advancing multi-modal language models with a comprehensive dataset and benchmark for chain-of-thought reasoning. In *Advances in Neural Information Processing Systems (NeurIPS)*, 2024a.
- Shao, Z., Wang, P., Zhu, Q., Xu, R., Song, J., Bi, X., Zhang, H., Zhang, M., Li, Y., Wu, Y., et al. Deepseekmath: Pushing the limits of mathematical reasoning in open language models. *arXiv preprint arXiv:2402.03300*, 2024b.
- Song, C. H., Blukis, V., Tremblay, J., Tyree, S., Su, Y., and Birchfield, S. Robospacial: Teaching spatial understanding to 2d and 3d vision-language models for robotics. In *Conference on Computer Vision and Pattern Recognition (CVPR)*, 2025.
- Tan, H., Ji, Y., Hao, X., Lin, M., Wang, P., Wang, Z., and Zhang, S. Reason-rft: Reinforcement fine-tuning for visual reasoning. In *Advances in Neural Information Processing Systems (NeurIPS)*, 2025.
- Team, G., Anil, R., Borgeaud, S., Wu, Y., Alayrac, J.-B., Yu, J., Soricut, R., Schalkwyk, J., Dai, A. M., Hauth, A., et al. Gemini: a family of highly capable multimodal models. *arXiv preprint arXiv:2312.11805*, 2023.
- Team, G. R., Abeyruwan, S., Ainslie, J., Alayrac, J.-B., Arenas, M. G., Armstrong, T., Balakrishna, A., Baruch, R., Bauza, M., Blokzijl, M., et al. Gemini robotics: Bringing ai into the physical world. *arXiv preprint arXiv:2503.20020*, 2025a.
- Team, K., Du, A., Gao, B., Xing, B., Jiang, C., Chen, C., Li, C., Xiao, C., Du, C., Liao, C., et al. Kimi k1.5: Scaling reinforcement learning with llms. *arXiv preprint arXiv:2501.12599*, 2025b.
- Wang, H., Zhao, Y., Wang, T., Fan, H., Zhang, X., and Zhang, Z. Ross3d: Reconstructive visual instruction tuning with 3d-awareness. In *International Conference on Computer Vision (ICCV)*, 2025a.
- Wang, J., Chen, M., Karaev, N., Vedaldi, A., Rupprecht, C., and Novotny, D. Vggt: Visual geometry grounded transformer. In *Conference on Computer Vision and Pattern Recognition (CVPR)*, 2025b.
- Wang, Q., Yu, Y., Yuan, Y., Mao, R., and Zhou, T. Videorf: Incentivizing video reasoning capability in mllms via reinforced fine-tuning. In *Advances in Neural Information Processing Systems (NeurIPS)*, 2025c.
- Wang, T., Mao, X., Zhu, C., Xu, R., Lyu, R., Li, P., Chen, X., Zhang, W., Chen, K., Xue, T., et al. Embodiedscan: A holistic multi-modal 3d perception suite towards embodied ai. In *Proceedings of the IEEE/CVF Conference on Computer Vision and Pattern Recognition*, pp. 19757–19767, 2024.
- Wang, Y., Ke, L., Zhang, B., Qu, T., Yu, H., Huang, Z., Yu, M., Xu, D., and Yu, D. N3d-vlm: Native 3d grounding enables accurate spatial reasoning in vision-language models. *arXiv preprint arXiv:2512.16561*, 2025d.
- Wen, X., Liu, Z., Zheng, S., Ye, S., Wu, Z., Wang, Y., Xu, Z., Liang, X., Li, J., Miao, Z., et al. Reinforcement learning with verifiable rewards implicitly incentivizes correct reasoning in base llms. *arXiv preprint arXiv:2506.14245*, 2025.
- Wu, D., Liu, F., Hung, Y.-H., and Duan, Y. Spatial-mllm: Boosting mllm capabilities in visual-based spatial intelligence. In *Advances in Neural Information Processing Systems (NeurIPS)*, 2025a.
- Wu, J., Guan, J., Feng, K., Liu, Q., Wu, S., Wang, L., Wu, W., and Tan, T. Reinforcing spatial reasoning in vision-language models with interwoven thinking and visual drawing. In *Advances in Neural Information Processing Systems (NeurIPS)*, 2025b.
- Wu, W., Mao, S., Zhang, Y., Xia, Y., Dong, L., Cui, L., and Wei, F. Mind’s eye of llms: visualization-of-thought elicits spatial reasoning in large language models. In *Advances in Neural Information Processing Systems (NeurIPS)*, 2024.
- Xu, R., Wang, X., Wang, T., Chen, Y., Pang, J., and Lin, D. Pointllm: Empowering large language models to understand point clouds. In *European Conference on Computer Vision (ECCV)*, 2024.
- Xu, R., Wang, W., Tang, H., Chen, X., Wang, X., Chu, F.-J., Lin, D., Feiszli, M., and Liang, K. J. Multi-spatialmllm: Multi-frame spatial understanding with multi-modal large language models. *arXiv preprint arXiv:2505.17015*, 2025.
- Yang, J., Chen, X., Qian, S., Madaan, N., Iyengar, M., Fouhey, D. F., and Chai, J. Llm-grounder: Open-vocabulary 3d visual grounding with large language model as an agent. In *International Conference on Robotics and Automation (ICRA)*, 2024.
- Yang, J., Yang, S., Gupta, A. W., Han, R., Fei-Fei, L., and Xie, S. Thinking in space: How multimodal large language models see, remember, and recall spaces. In

- Conference on Computer Vision and Pattern Recognition (CVPR)*, 2025a.
- Yang, R., Zhu, Z., Li, Y., Huang, J., Yan, S., Zhou, S., Liu, Z., Li, X., Li, S., Wang, W., et al. Visual spatial tuning. *arXiv preprint arXiv:2511.05491*, 2025b.
- Yang, S., Yang, J., Huang, P., Brown, E., Yang, Z., Yu, Y., Tong, S., Zheng, Z., Xu, Y., Wang, M., et al. Cambrian-s: Towards spatial supersensing in video. *arXiv preprint arXiv:2511.04670*, 2025c.
- Yeshwanth, C., Liu, Y.-C., Nießner, M., and Dai, A. Scan-net++: A high-fidelity dataset of 3d indoor scenes. In *International Conference on Computer Vision (ICCV)*, 2023.
- Yin, B., Wang, Q., Zhang, P., Zhang, J., Wang, K., Wang, Z., Zhang, J., Chandrasegaran, K., Liu, H., Krishna, R., et al. Spatial mental modeling from limited views. *arXiv preprint arXiv:2506.21458*, 2025.
- Yu, Q., Zhang, Z., Zhu, R., Yuan, Y., Zuo, X., Yue, Y., Dai, W., Fan, T., Liu, G., Liu, L., et al. Dapo: An open-source llm reinforcement learning system at scale. In *Advances in Neural Information Processing Systems (NeurIPS)*, 2025a.
- Yu, S., Chen, Y., Ju, H., Jia, L., Zhang, F., Huang, S., Wu, Y., Cui, R., Ran, B., Zhang, Z., et al. How far are vlms from visual spatial intelligence? a benchmark-driven perspective. *arXiv preprint arXiv:2509.18905*, 2025b.
- Yuan, Y., Cui, H., Huang, Y., Chen, Y., Ni, F., Dong, Z., Li, P., Zheng, Y., and Hao, J. Embodied-r1: Reinforced embodied reasoning for general robotic manipulation. *arXiv preprint arXiv:2508.13998*, 2025a.
- Yuan, Z., Jiang, S., Feng, C.-M., Zhang, Y., Cui, S., Li, Z., and Zhao, N. Scene-r1: Video-grounded large language models for 3d scene reasoning without 3d annotations. *arXiv preprint arXiv:2506.17545*, 2025b.
- Yue, Y., Chen, Z., Lu, R., Zhao, A., Wang, Z., Song, S., and Huang, G. Does reinforcement learning really incentivize reasoning capacity in llms beyond the base model? In *Advances in Neural Information Processing Systems (NeurIPS)*, 2025.
- Zhan, X., Huang, W., Sun, H., Fu, X., Ma, C., Cao, S., Jia, B., Lin, S., Yin, Z., Bai, L., et al. Actial: Activate spatial reasoning ability of multimodal large language models. In *Advances in Neural Information Processing Systems (NeurIPS)*, 2025.
- Zhang, J., Wang, K., Xu, R., Zhou, G., Hong, Y., Fang, X., Wu, Q., Zhang, Z., and Wang, H. Navid: Video-based vlm plans the next step for vision-and-language navigation. *arXiv preprint arXiv:2402.15852*, 2024.
- Zhang, J., Chen, Y., Zhou, Y., Xu, Y., Huang, Z., Mei, J., Chen, J., Yuan, Y.-J., Cai, X., Huang, G., et al. From flatland to space: Teaching vision-language models to perceive and reason in 3d. In *Advances in Neural Information Processing Systems (NeurIPS)*, 2025a.
- Zhang, K., Li, B., Zhang, P., Pu, F., Cahyono, J. A., Hu, K., Liu, S., Zhang, Y., Yang, J., Li, C., et al. Lmms-eval: Reality check on the evaluation of large multimodal models. In *Findings of the Association for Computational Linguistics: NAACL*, 2025b.
- Zhang, Y., Wu, J., Li, W., Li, B., Ma, Z., Liu, Z., and Li, C. Video instruction tuning with synthetic data. *Transactions on Machine Learning Research (TMLR)*, 2025c.
- Zhao, B., Wang, Z., Fang, J., Gao, C., Man, F., Cui, J., Wang, X., Chen, X., Li, Y., and Zhu, W. Embodied-r: Collaborative framework for activating embodied spatial reasoning in foundation models via reinforcement learning. In *Proceedings of the 33rd ACM International Conference on Multimedia*, 2025.
- Zheng, C., Liu, S., Li, M., Chen, X.-H., Yu, B., Gao, C., Dang, K., Liu, Y., Men, R., Yang, A., et al. Group sequence policy optimization. *arXiv preprint arXiv:2507.18071*, 2025a.
- Zheng, D., Huang, S., Zhao, L., Zhong, Y., and Wang, L. Towards learning a generalist model for embodied navigation. In *Proceedings of the IEEE/CVF Conference on Computer Vision and Pattern Recognition*, pp. 13624–13634, 2024.
- Zheng, D., Huang, S., Li, Y., and Wang, L. Learning from videos for 3d world: Enhancing mllms with 3d vision geometry priors. In *Advances in Neural Information Processing Systems (NeurIPS)*, 2025b.
- Zheng, D., Huang, S., and Wang, L. Video-3d llm: Learning position-aware video representation for 3d scene understanding. In *Conference on Computer Vision and Pattern Recognition (CVPR)*, 2025c.
- Zheng, H., Li, S., Li, Y., and Yin, H. Spatialreasoner: Active perception for large-scale 3d scene understanding. *arXiv preprint arXiv:2512.03284*, 2025d.
- Zheng, H., Xiang, L., Yang, Q., Lin, Q., and Yin, H. Reg3d: Reconstructive geometry instruction tuning for 3d scene understanding. *arXiv preprint arXiv:2509.03635*, 2025e.
- Zhong, Y., Hu, Z.-Y., Li, Y., and Wang, L. Rethinking chain-of-thought reasoning for videos. *arXiv preprint arXiv:2512.09616*, 2025.

- Zhou, E., An, J., Chi, C., Han, Y., Rong, S., Zhang, C., Wang, P., Wang, Z., Huang, T., Sheng, L., et al. Roborefer: Towards spatial referring with reasoning in vision-language models for robotics. In *Advances in Neural Information Processing Systems (NeurIPS)*, 2025.
- Zhu, C., Wang, T., Zhang, W., Pang, J., and Liu, X. Llava-3d: A simple yet effective pathway to empowering llms with 3d-awareness. In *International Conference on Computer Vision (ICCV)*, 2025a.
- Zhu, F., Wang, H., Xie, Y., Gu, J., Ding, T., Yang, J., and Jiang, H. Struct2d: A perception-guided framework for spatial reasoning in large multimodal models. In *Advances in Neural Information Processing Systems (NeurIPS)*, 2025b.
- Zhu, J., Wang, W., Chen, Z., Liu, Z., Ye, S., Gu, L., Tian, H., Duan, Y., Su, W., Shao, J., et al. Internvl3: Exploring advanced training and test-time recipes for open-source multimodal models. *arXiv preprint arXiv:2504.10479*, 2025c.
- Zhu, Z., Ma, X., Chen, Y., Deng, Z., Huang, S., and Li, Q. 3d-vista: Pre-trained transformer for 3d vision and text alignment. In *International Conference on Computer Vision (ICCV)*, 2023.
- Zhu, Z., Zhang, Z., Ma, X., Niu, X., Chen, Y., Jia, B., Deng, Z., Huang, S., and Li, Q. Unifying 3d vision-language understanding via promptable queries. In *European Conference on Computer Vision (ECCV)*, 2024.

A. Implementation Details

A.1. Data

3D Video Detection. For 3D video detection, we re-use the data from VG LLM (Zheng et al., 2025b), which was initially curated from EmbodiedScan (Wang et al., 2024). The data comprises consecutive frames and the corresponding visible object annotations in indoor scenes, covering 958 scenes for training and 243 scenes for evaluation. The object 3D bounding boxes are transformed to the coordinate system of the first frame.

3D Visual Grounding. We use the ScanRefer (Chen et al., 2020) dataset for 3D visual grounding, which is a common practice. ScanRefer includes 37K pairs of object grounding text and axis-aligned 3D bounding boxes across 562 indoor scans. We follow prior works (Zhang et al., 2025a; Zheng et al., 2025b) in terms of spatio-temporal grounding formulation and data processing procedures.

3D Spatial Reasoning. Our SFT data for the spatial reasoning task includes VSI-207K from VLM-3R (Fan et al., 2025) and Sr-91K from SpaceR (Ouyang et al., 2025), spanning ScanNet (Dai et al., 2017), ScanNet++ (Yeshwanth et al., 2023), and ARKitScenes (Baruch et al., 2021). Our CoT data is generated by Qwen3-VL-32B-Thinking (Bai et al., 2025a) and curated by selecting those whose accuracy rewards exceed 0.85. The curated CoT-10K comprises 9.2K from VLM-3R-VSI subset (Fan et al., 2025) and 0.8K from SQA3D (Ma et al., 2023).

A.2. Training

Training Settings. All experiments are conducted on 8 Nvidia A100 GPUs. For the 3D video detection and 3D visual grounding tasks, we adopt the full fine-tuning strategy following the settings in VG LLM. In contrast, for 3D spatial reasoning, we employ LoRA (Hu et al., 2022) and set the KL-Divergence penalty coefficient to zero during policy training.

GPU Memory Bottleneck in 3D-RFT. A critical bottleneck in video-based 3D scene understanding tasks is the prohibitive GPU memory consumption required by GRPO. The necessity of maintaining a large group size leads to substantial memory spikes. Specifically, processing long-context video inputs with high-resolution vision encoders (e.g., VGGT) generates extensive computation graphs. In standard implementations, storing activations for all K samples simultaneously often exceeds VRAM capacity, resulting in Out-Of-Memory (OOM) errors.

Loss Backward Chunking. To mitigate this, we introduce a gradient accumulation strategy that partitions the global batch indices $\{1, \dots, K\}$ into M disjoint micro-chunks $\{C_1, \dots, C_M\}$. The size of each chunk is constrained such that $|C_m| \leq M_{\text{micro}}$ to fit within GPU memory limits. Accordingly, we reformulate the total loss as a sum of chunked losses:

$$\mathcal{L}_{\text{chunked}}(\theta) = \sum_{m=1}^M \frac{|C_m|}{K} \mathcal{L}_{C_m}(\theta), \quad (15)$$

$$\text{where } \mathcal{L}_{C_m}(\theta) = \frac{1}{|C_m|} \sum_{k \in C_m} \sum_t \mathcal{L}_{k,t}(\theta). \quad (16)$$

By iteratively computing and accumulating gradients for each \mathcal{L}_{C_m} , we reduce the peak memory complexity from $\mathcal{O}(B \times G)$ to $\mathcal{O}(M_{\text{micro}})$. This approach enables significant scaling of the group size G without hurting the training performance. In our experiments, we set the micro-chunk size to 2 for 3D video detection, 4 for 3D visual grounding, and 1 for 3D spatial reasoning.

B. Additional Results

B.1. Qualitative Results

B.1.1. 3D VIDEO DETECTION

The qualitative results for 3D video detection in Fig. 10 corroborate our quantitative analysis, highlighting the enhanced precision of 3D-RFT. Consistent with the reduction in false positives reported in Tab. 1, 3D-RFT-4B successfully avoids the hallucinations generated by the baseline. For instance, in the first row, VG LLM-4B misinterprets a curtain’s shadow as a valid box, and in the second row, it hallucinates a table on the floor; our model correctly suppresses both errors. Furthermore, 3D-RFT-4B demonstrates superior semantic granularity and recall: in the last row, it precisely classifies “toilet paper”

RFT for 3D Scene Understanding

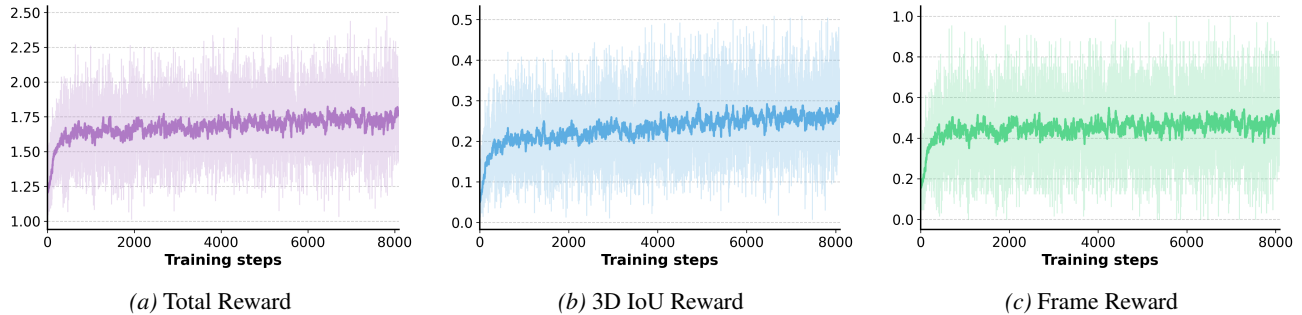


Figure 8. **Training Dynamics of 3D Visual Grounding.** We visualize the training curves for the total reward (left), the 3D IoU reward (middle), and the Frame Alignment reward (right). The curves show stable convergence and correlation with the optimization objectives.

(improving upon the baseline’s coarser label “paper”), and in the third row, it successfully detects a “desk” that the baseline misses.

B.1.2. 3D VISUAL GROUNDING

In Fig. 11, we provide qualitative results of 3D visual grounding. The evaluation is conducted under a 32-frame setting, and we choose some key frames manually for visualization.

B.1.3. 3D SPATIAL REASONING

We present qualitative results for 3D spatial reasoning in Sec. C.2. In these cases, we sample some frames from the raw video. These examples demonstrate that 3D-RFT-4B is capable of generating concise, scene-grounded CoT reasoning to facilitate accurate answer prediction.

B.2. Training Dynamics of 3D Visual Grounding

We illustrate the training dynamics of 3D visual grounding in Fig. 8. The curves demonstrate a consistent upward trend for both the frame reward and the 3D IoU reward, indicating a stable and effective optimization process.

C. Discussion

C.1. Impact of TA Data for SFT

We compare the OOD evaluation results of SFT (DA) and SFT (DA+TA) on MindCube-Tiny (Yin et al., 2025). The results in Fig. 9 show that SFT (DA) significantly lags behind SFT (DA+TA) under both TA and DA test settings. SFT (DA) also shows notable performance drops compared to the vanilla Qwen2.5-VL-3B baseline. This indicates the potential overfitting issues in training 3D MLLM with solely DA data, appealing for mixing more TA data (*i.e.*, CoT data) for comprehensive enhancement of MLLM’s capabilities.

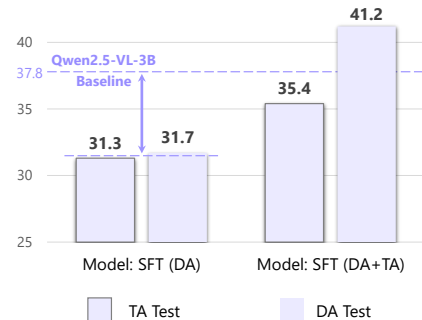


Figure 9. **Evaluation results on MindCube-Tiny.**

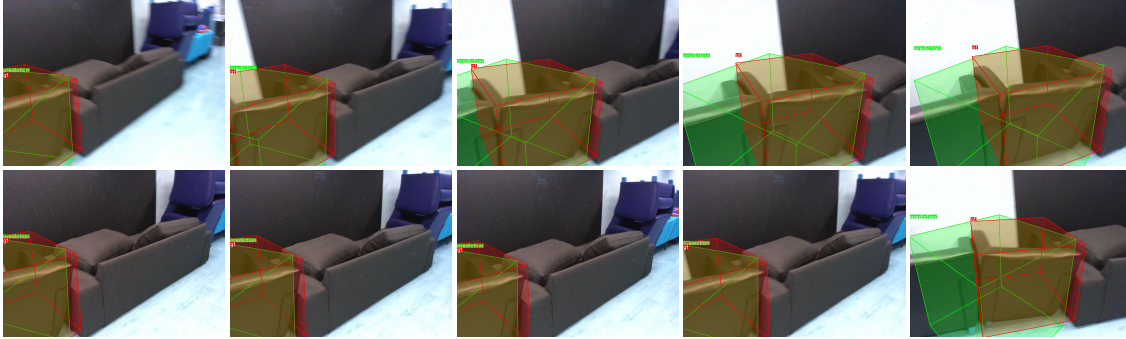
C.2. Remarks

Unlike domains where RLVR thrives (*e.g.*, math and coding), 3D scene understanding presents distinct challenges. First, the scarcity of high-quality labels and the inherent sparsity of learning signals constitute major obstacles. The cost and difficulty of 3D CoT data collection further hinder the efficacy of RLVR for 3D scene understanding. Our findings suggest that RLVR outcomes are sensitive to CoT data quality, highlighting the refinement of CoT data as a critical future direction. Second, while math and coding tasks exhibit a straightforward reasoning loop within a unified textual modality, 3D scene understanding requires robust 3D-aware perception from video inputs before reasoning can occur. This perceptual stage represents a significant bottleneck, which could undermine the correctness and coherence of the model’s thoughts. Therefore, future research should prioritize process reward designs to guarantee the soundness of reasoning within 3D scenes.



Figure 10. Qualitative comparison of 3D object detection (20 common classes) results. We compare the predictions of the baseline VG LLM-4B against our 3D-RFT-4B model.

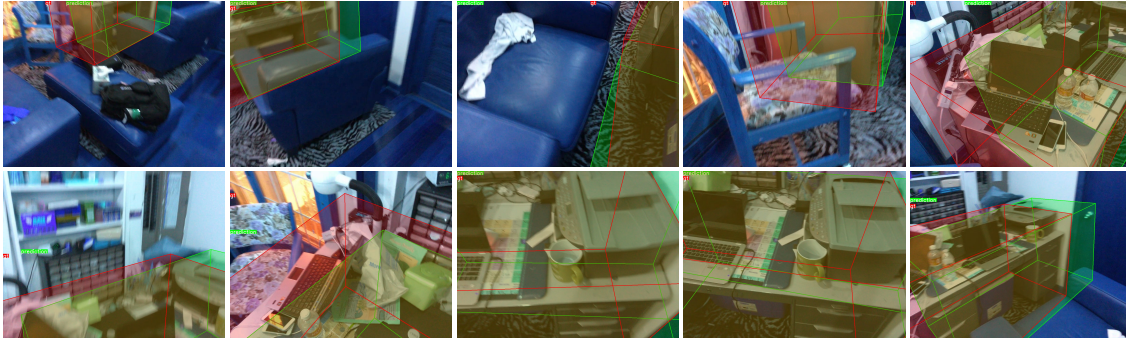
Grounding Text: “There are two black chairs situated between six brown chairs and a black couch. this black chair is next to the black couch. it appears to be leather. it is black. there is a snack machine on the opposite wall.”



Grounding Text: “A black top located in center of desk. the lid is open and blue screen is visible.”



Grounding Text: “The brown desk is right next to the window by the chair. the desk is also right in front of the door.”



Grounding Text: “This is a black table. it is to the right of the kitchen cabinet.”

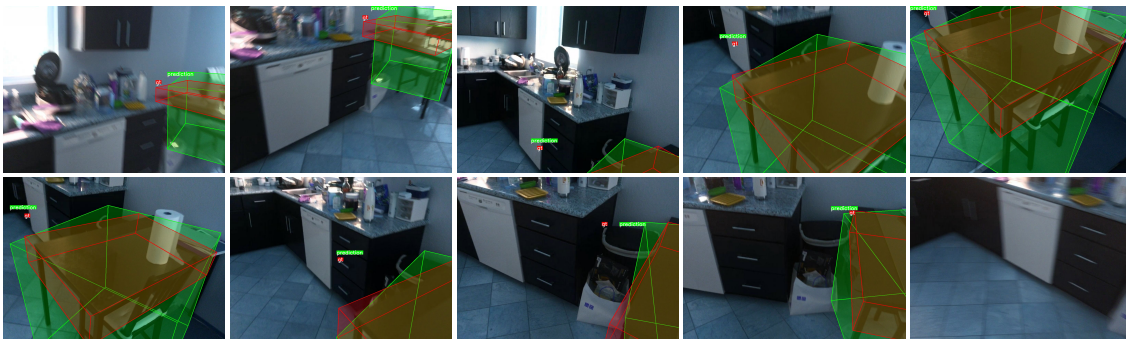


Figure 11. Qualitative results of 3D Visual Grounding using our 3D-RFT-4B. Each block shows the grounding text followed by 10 video frames visualizing the predicted 3D bounding boxes (green) and ground truth (red).

Video



Question

These are frames of a video. Measuring from the closest point of each object, what is the distance between the stool and the washer (in meters)?

3D-RFT-4B

<think>

The stool is near the table and the washer is in the lower part of the kitchen area.

</think>

<answer>1.4</answer> **GT: 1.3**

Figure 12. Qualitative example on VSI-Bench (absolute distance).

Video



Question

These are frames of a video. If I am standing by the stove and facing the refrigerator, is the table to my front-left, front-right, back-left, or back-right? The directions refer to the quadrants of a Cartesian plane (if I am standing at the origin and facing along the positive y-axis).

Options: A. front-right B. front-left C. back-left D. back-right

3D-RFT-4B

<think>

I am standing by the stove, which is on the left side of the kitchen. The refrigerator is on the right side of the kitchen. The table is located in the middle of the kitchen, to the right of the refrigerator.

</think>

<answer>A</answer> **GT: A**

Figure 13. Qualitative example on VSI-Bench (relative direction).

Video



Question

These are frames of a video. You are a robot beginning at the door and facing the desk. You want to navigate to the window. You will perform the following actions (Note: for each [please fill in], choose either “turn back,” “turn left,” or “turn right.”): 1. Go forward until the desk 2. [please fill in] 3. Go forward until the bed 4. [please fill in] 5. Go forward until the window. You have reached the final destination. Options: A. Turn Right, Turn Right B. Turn Right, Turn Left C. Turn Back, Turn Right D. Turn Left, Turn Left

3D-RFT-4B

<think>

The robot starts at the door facing the desk. To reach the window, it must first go forward to the desk, then turn right to face the bed, and finally turn right again to reach the window.

</think>

<answer>B</answer> **GT: B**

Figure 14. Qualitative example on VSI-Bench (route plan).

D. Limitations

In this work, we focus on demonstrating the efficacy of the RFT paradigm by conducting task-specific fine-tuning during the RL stage; we do not currently explore unified, multi-task fine-tuning. Consequently, investigating how to balance diverse task rewards to enable efficient mixed training remains a critical direction for future research. Furthermore, we do not utilize CoT data for 3D perception tasks due to the challenges associated with collecting high-quality reasoning annotations in this domain. Acquiring such data and analyzing the impact of CoT on perception capabilities represents another promising avenue for advancing video-based 3D scene understanding models.